Chapter

Atomic Dynamics in Real Space and Time

Takeshi Egami

Abstract

Atomic and molecular dynamics in strongly disordered matter, such as liquid, cannot be fully described in terms of phonons, because they are marginalized and often overdamped. Their dynamic and transport properties depend on local atomic rearrangements which are strongly correlated. To describe such local dynamics, the usual representation in momentum (Q) and energy (E) space in terms of the dynamic structure factor, $S(Q, E)$, is not effective. We discuss an alternative approach in real space (r) and time (t), with the van Hove function, $G(r, t)$, and show how this approach facilitates understanding of real-space local dynamics of liquids and other disordered systems in the length scale of Å and time scale of pico-second.

Keywords: local atomic dynamics, van Hove function, liquid, glass, correlated dynamics

1. Introduction

In crystalline solids, phonons are the elementary excitations of lattice dynamics. They can be observed with well-defined dispersions in the dynamic structure factor, $S(\boldsymbol{Q}, E)$, where $\boldsymbol{Q}$ is the momentum exchange and E ($= \hbar\omega$) is the energy exchange in scattering. The $S(\boldsymbol{Q}, E)$ can be measured by inelastic X-ray scattering (IXS) as discussed in this book or by inelastic neutron scattering (INS). However, in strongly disordered materials, shortwave phonons have very short mean free path and lifetime. Only long-wave phonons, for which the atomic structure is irrelevant and the material acts as a continuum elastic body, propagate over some distance. However, the total spectral weight of long-wave phonons is small, because the phonon density of states increases as E^2. For this reason, a majority of phonons are overdamped, and some of them are localized, particularly in liquid.

Atomic dynamics in liquid and soft matter is usually studied by quasi-elastic scattering (QES) at low Q, where the QES intensity is dominated by the self-correlation and the auto-correlation of the same atom. The energy width of QES is proportional to DQ^2, where D is the diffusion constant. For hydrogen, which has a very large incoherent cross section, the value of D determined by QES at low Q is the isotopic diffusivity, D_i, determined by the diffusion profile of isotopes measured by sectioning. The chemical diffusivity, D_c, which characterizes the flow of elements responding to concentration gradient, is usually different from D_i, because of the backflow of diffusing atoms. The ratio, $f = D_c/D_i$, is known as the correlation factor and describes how diffusive atomic jumps are correlated.

This example illustrates the importance of studying the distinct atomic correlation and the dynamic correlation among different atoms. The importance of knowing the distinct terms of the correlation function is beginning to be recognized [1, 2], but the difficulty of measurement delayed advances. Only recently the progress in IXS instrumentation [3, 4] and the advent of pulsed neutron sources [5] made it feasible to measure $S(Q, E)$ over wide ranges of Q and E in a reasonable time and opened the possibility of garnering information on distinct atomic correlations.

Conversely, even though the substantial progress in instrumentation allowed us to collect a much larger amount of data which contain vastly richer information, the IXS data are mostly processed in the same way, just by focusing on the phonon dispersion and its width [6]. Similarly, usually only the diffusivity is obtained from the QES data. What is missing is the analysis of the *diffuse* IXS intensity which is usually discarded as background. This situation is a perfect analog of the structural analysis of disordered crystals. The conventional methods of crystallographic analysis focus only on the Bragg peaks, and the diffuse scattering intensity is processed separately to determine the short-range order. However, by combining the Bragg and diffuse intensities as the total scattering intensity and Fourier-transforming it into the atomic pair distribution function (PDF), precise local structural information can be obtained [7]. In the same manner, by including the diffuse IXS intensity, valuable information on local dynamics can directly be obtained.

2. Van Hove function

2.1 Definition

After the correction for absorption and normalization, the IXS intensity, $I(Q, E)$, is reduced to $S(Q, E)$ [8],

$$S(\mathbf{Q}, E) = \frac{1}{2\pi\hbar N} \sum_{i,j} \int \left\langle \exp\left[\mathbf{Q} \cdot \left(\mathbf{r_i}(0) - \mathbf{r_j}(t)\right)\right] \right\rangle \exp\left(-\frac{E}{\hbar} t\right) dt, \tag{1}$$

where $\boldsymbol{r_i}(t)$ is the position of the atom i at time t. It is useful to separate it into the self-part ($i = j$), $S_s(\mathbf{Q}, E)$, and the distinct-part ($i \neq j$), $S_d(\mathbf{Q}, E)$.

$$S(\mathbf{Q}, E) = S_s(\mathbf{Q}, E) + S_d(\mathbf{Q}, E). \tag{2}$$

For isotropic matter such as liquid, we use the spherical average,

$$S(Q, E) = \frac{1}{4\pi} \int S(\mathbf{Q}, E) d\Omega, \tag{3}$$

where $Q = |\boldsymbol{Q}|$ and Ω is the solid angle in Q space. Upon the Fourier transformation into the time-domain, we obtain the intermediate scattering function [8],

$$F(Q, t) = \int S(Q, E) \exp\left(i \frac{E}{\hbar} t\right) dE, \tag{4}$$

which has been widely used in the analysis of soft matter dynamics [9–11]. Another step of the Fourier transformation, this time from momentum space to real space, leads to the van Hove function [12],

$$G(r,t) = 1 + \frac{1}{2\pi^2\rho_0 r}\int F(Q,t)\sin(Qr)QdQ$$
$$= \frac{1}{4\pi\rho_0 N r^2}\sum_{i,j}\delta\left(r - \left|\mathbf{r}_i(0) - \mathbf{r}_\mathbf{j}(t)\right|\right). \tag{5}$$

Again it is useful to divide it into the self-part, $G_s(r, t)$, and the distinct-part, $G_d(r, t)$. Although the van Hove function has been known for a long time, its experimental determination has rarely been done [13] because it requires $S(Q, E)$ to be known over wide ranges of Q and E. Only recently it became practical [14, 15] because of the progress in instrumentation as noted above and discussed below.

In the regular X-ray diffraction measurement, the energy resolution is of the order of 1 eV, far greater than the phonon excitation energies. Therefore what is measured is the energy-integrated intensity,

$$S(Q) = \int S(Q,E)dE, \tag{6}$$

which leaves only the same-time (t = 0) contribution in Eq. (1). Therefore its Fourier transform, the PDF,

$$g(r) = 1 + \frac{1}{2\pi^2\rho_0 r}\int [S(Q) - 1]\sin(Qr)QdQ, \tag{7}$$

is equal to $G(r, 0)$. In other words the van Hove function describes how the PDF, the snapshot correlation function, decays with time.

2.2 Evolution with time

At a short time scale (~0.1 ps), atomic motions are ballistic, but after atoms leave the neighbor cage, they become diffusive. Then the self-term of the van Hove function in the diffusive regime should be

$$G_s(r,t) = \frac{1}{\rho_0}\left(\frac{1}{4\pi D_i t}\right)^{\frac{3}{2}}\exp\left(-\frac{r^2}{4D_i t}\right). \tag{8}$$

Therefore the self-diffusion coefficient, D_i, can be determined from the self-part of the van Hove function. The double Fourier transform of Eq. (8) is

$$S_s(Q,\omega) = \frac{D_i Q^2/\pi}{\omega^2 + \left(D_i Q^2\right)^2}, \tag{9}$$

which can be measured by QES and is routinely used for determining D_i. In the case of quasi-elastic neutron scattering (QENS) from hydrogen, because the incoherent cross section of hydrogen is so large, the scattering intensity is totally dominated by $S_s(Q, \omega)$, and the measurement readily yields the value of D_i. In general, however, there can be some contributions from the distinct-part to the low-angle QES, which can make the measurement inaccurate. On the other hand in the van Hove function the self-part is cleanly separated, at least initially, resulting in more accurate determination of D_i.

The decay of the first peak of the PDF with time describes how the nearest neighbor shell of an atom, known as the first-neighbor cage, disintegrates with

time. The van Hove function depicts this decay nicely and can relate the time scale of decay to the topological relaxation time and to viscosity as shown below.

The early prediction on the distinct-part of the van Hove function was that it could be expressed by the convolution of the PDF by the self-part (Eq. (8)) [16]. Then the QES width should be equal to DQ^2, by Eq. (9). But de Gennes noted that QES becomes anomalously narrow in the vicinity of the first peak in $S(Q)$ [17]. He suggested that this phenomenon, now known as the de Gennes narrowing, was due to the collective nature of the dynamics represented by the first peak in $S(Q)$. Since then it became customary to equate the observation of the de Gennes narrowing to the confirmation of collective excitations. A recent study [18], however, showed otherwise. It was found that even in high-temperature liquid, in which atomic motions are uncorrelated, the decay time of $G(r, t)$ depends linearly on distance. In general,

$$\tau(r) = \tau_0 + \tau_r \left(\frac{r}{r_1}\right)^{\chi}, \tag{10}$$

where r_1 is the position of the nearest neighbor peak of the PDF. As shown in **Figure 1**, the exponent χ depends on dimensionality d approximately as $\chi = (d\text{-}1)/2$; thus $\chi = 1$ for three dimensions. This is because at large r, each PDF peak describes not just one atomic distance but many. Therefore its decay with time does not correspond to the single atom dynamics. The number of pairs of atoms in each peak, N_r, is proportional to the surface area, $4\pi r^{d-1}$. Then its fluctuation is proportional to $\sqrt{N_r} \sim r^{(d-1)/2}$; therefore $\chi = (d\text{-}1)/2$. Now the first peak of $S(Q)$ represents the medium-range part of the PDF, beyond the first peak [19], so its decay is slow, reflecting the behavior of the PDF beyond the first peak. This argument proves that the de Gennes narrowing does not necessary imply collective excitations but can be just the natural consequence of geometry.

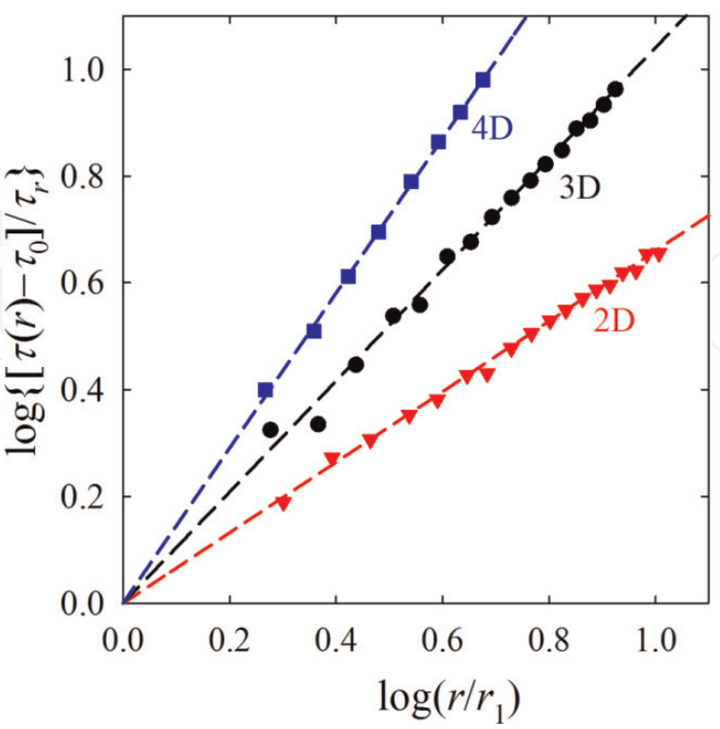

Figure 1.
The r-dependent relaxation time τ(r) for model liquid iron in 2D (red triangle) χ = 0.66, 3D (black circle) χ = 1.04, and 4D χ = 1.45, beyond the first peak. The data points are shown in the form of log{[τ(r)-τ0]/τr} versus log(r/r1) to highlight χ from the expected power law dependence. The short dashed lines serve as guides to the eye [18].

3. Local dynamics of water and aqueous solution of salt

3.1 Van Hove function of water

Figure 2 shows the $S(Q, E)$ of water at room temperature, determined by the IXS experiment at the beam line XL35 of the SPring-8 facility [14]. Earlier IXS experiments to observe phonons did not cover the Q space much beyond 1 $Å^{-1}$ [6, 20, 21]. The $S(Q, E)$ is dominated by QES, and as is given it is not easy to garner useful information without extensive modeling. Converting the data into the van Hove function makes local dynamics directly visible as shown in **Figure 3**. Because hydrogen is almost invisible to X-rays, the van Hove function is dominated by oxygen–oxygen correlation. To minimize the termination error for stopping the integration by Eq. (4) at a maximum Q value, $F(Q, t)$ can be extended to large Q

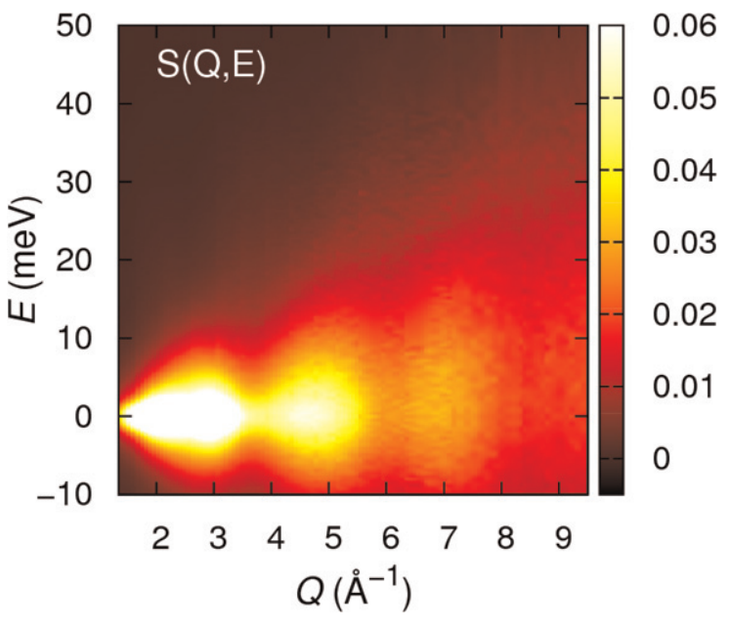

Figure 2.
The S(Q, E) of water at room temperature, determined by the IXS experiment at the beam line XL35 of the SPring-8 facility [14].

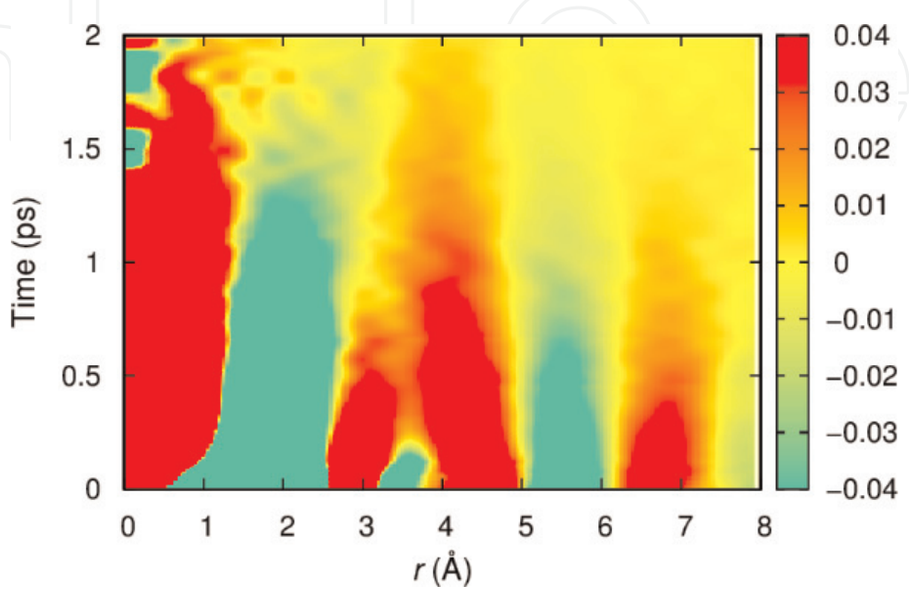

Figure 3.
The van Hove function of water [14].

by adding $S(Q)$ exp.$(-D(Q)Q^2t)$, which is justified for the self-correlation function [14].

In **Figure 3** the data at t = 0 is the snapshot PDF which can be obtained by the conventional diffraction measurement. At t = ∞ $G(r, \infty)$ = 1, so that $G(r, t)$ - 1 describes the correlation. The decay of the PDF to $G(r, \infty)$ = 1 is not uniform, with each peak behaving in different ways. In particular the first peak moves away, while the second peak moves in, indicating that the local dynamics is highly correlated. As the nearest neighbor moves away, the second neighbor comes in to take its place to maintain the coordination unchanged. The area of the first peak above $G(r, t)$ = 1 shows a two-step decay,

$$A(t) = A_1 e^{-(t/\tau_1)^{\gamma_1}} + A_2 e^{-(t/\tau_2)^{\gamma_2}}. \quad (11)$$

The first term (τ_1 = 0.32 ps) describes the ballistic motion of the atom, whereas the second term with the temperature-dependent τ_2 describes the change in molecular bond. Earlier through molecular dynamics (MD) simulations, it was found that the time scale of losing one nearest neighbor, τ_{LC}, is directly related to viscosity through $\tau_{LC} = \tau_M = \eta/G_\infty$, where τ_M is the Maxwell relaxation time, η is viscosity, and G_∞ is instantaneous shear modulus [22]. By relating τ_2 to τ_{LC} through simulation (for water $\tau_2 = \tau_{LC}$), this relationship was proven for water [14, 23].

3.2 Self-diffusion

The portion of the van Hove function near r = 0 describes the self-correlation, $G_s(r, t)$. Indeed it follows Eq. (8) quite well for water as shown in **Figure 4** [24].

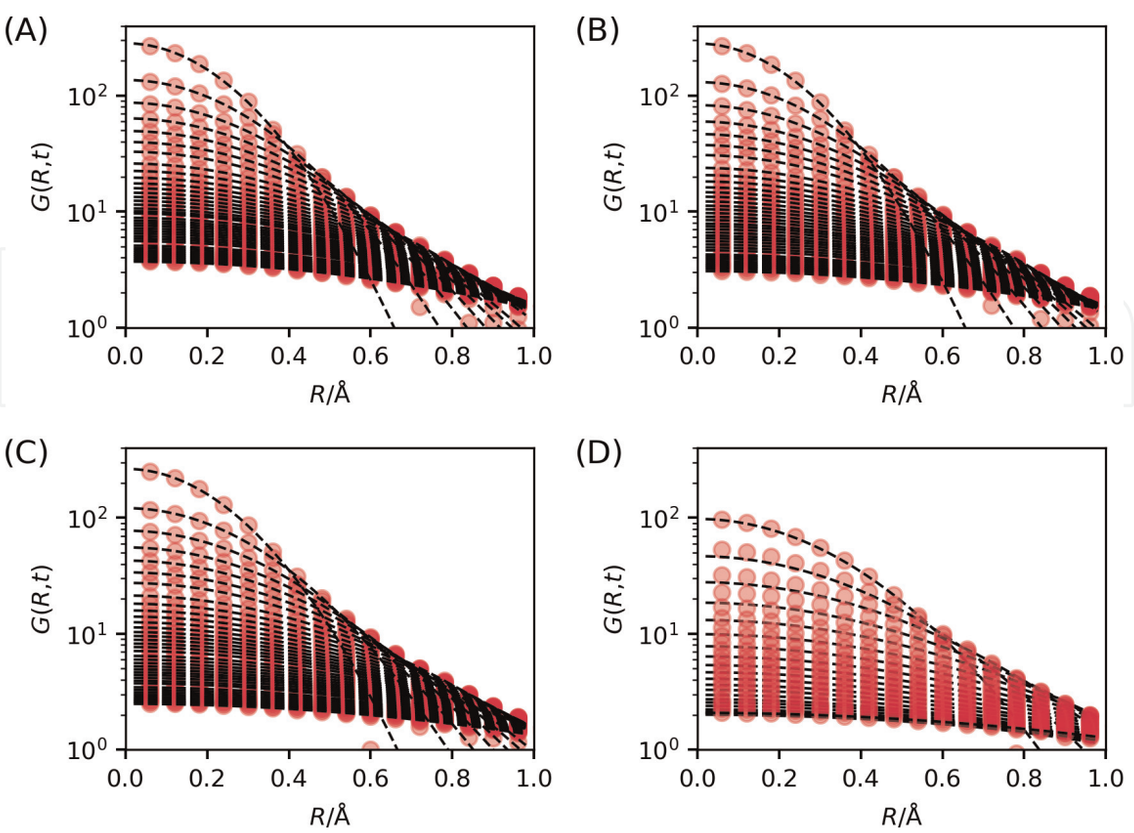

Figure 4.
The self-part of the van Hove function for water at (A) 285 K, (B) 295 K, (C) 310 K, and (D) 318 K. (circles) experimental data and (dashed line) the result of fitting by Eq. (8).

However, the values of diffusivity determined from Eq. (8) vary from the values obtained by other methods [24]. The origin of this discrepancy is yet to be determined.

3.3 Van Hove function of salty water

About 70% of the earth is covered by salty water, and 80% our body is also made of salty water. Therefore it is important to know how salt affects the properties of

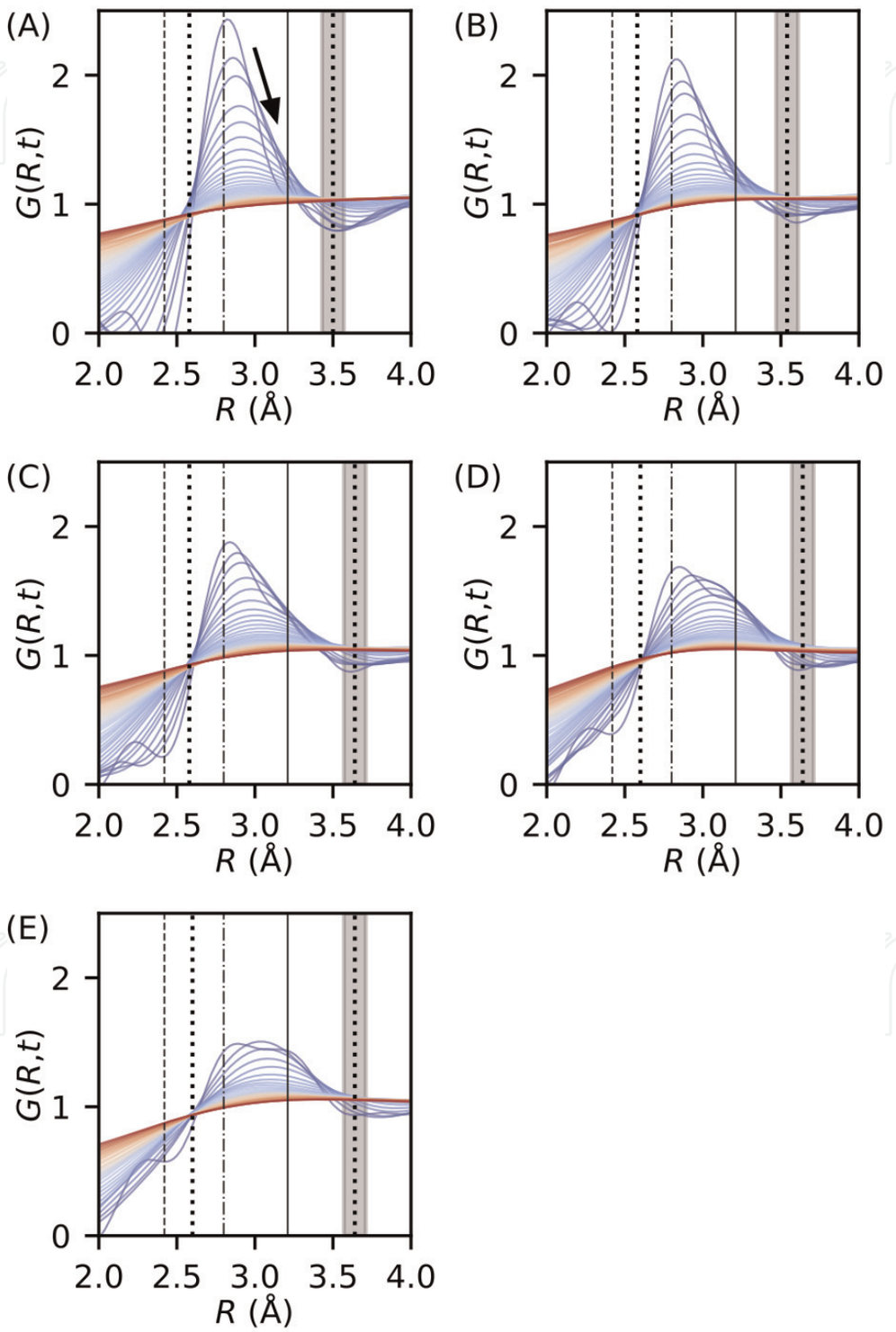

Figure 5.
The van Hove functions around the first-neighbor correlation peak, R ~ 2.9 Å: (A) pure water, (B) m = 0.75 mol/kg, (C) 1.5 mol/kg, (D) 2.26 mol/kg, and (E) 3.0 mol/kg. The solid lines at R = 3.21 Å show the R_{O_2-} + R_{Cl-}. The dashed line at R = 2.42 Å shows the R_{O_2-} + R_{Na+}. The dash-dotted line at R = 2.8 Å shows the R_{O_2-} + R_{O_2-}. The range between the dotted lines ($\mathbf{R_1}'$ and $\mathbf{R_1}''$) was used to calculate the area, A(t), of the first neighbor. The upper limit of this range is changed within the gray-shaded area to estimate the uncertainties [25].

water, such as viscosity. We studied the local dynamics of aqueous solution of NaCl up to 2 mol/kg by IXS [24] using the BLX-43 beam line of SPring-8 which has as many as 24 analyzer crystals. With this setup a dataset similar to that shown in **Figure 2** can be collected in 12 h.

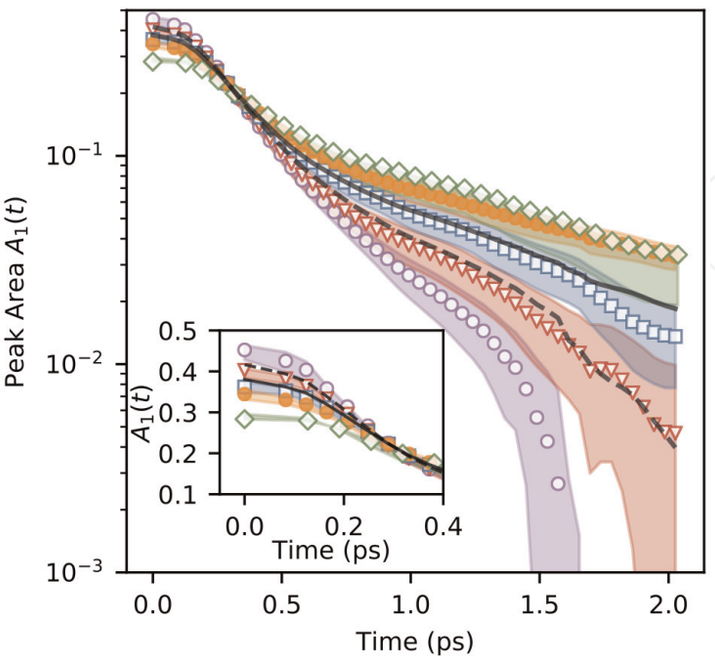

Figure 6.
Temporal evolution in the area of the first-neighbor peak, $A_1(t)$, and the enlarged view (inset): (open circles) pure water, (triangles) m = 0.75 mol/kg, (squares) 1.5 Mol/kg, (closed circles) 2.26 mol/kg, and (diamonds) 3.0 mol/kg. The shaded areas represent uncertainties of each dataset. The solid and dashed lines represent the linear combination of time evolution for m = 0 and 2.26 mol/kg [25].

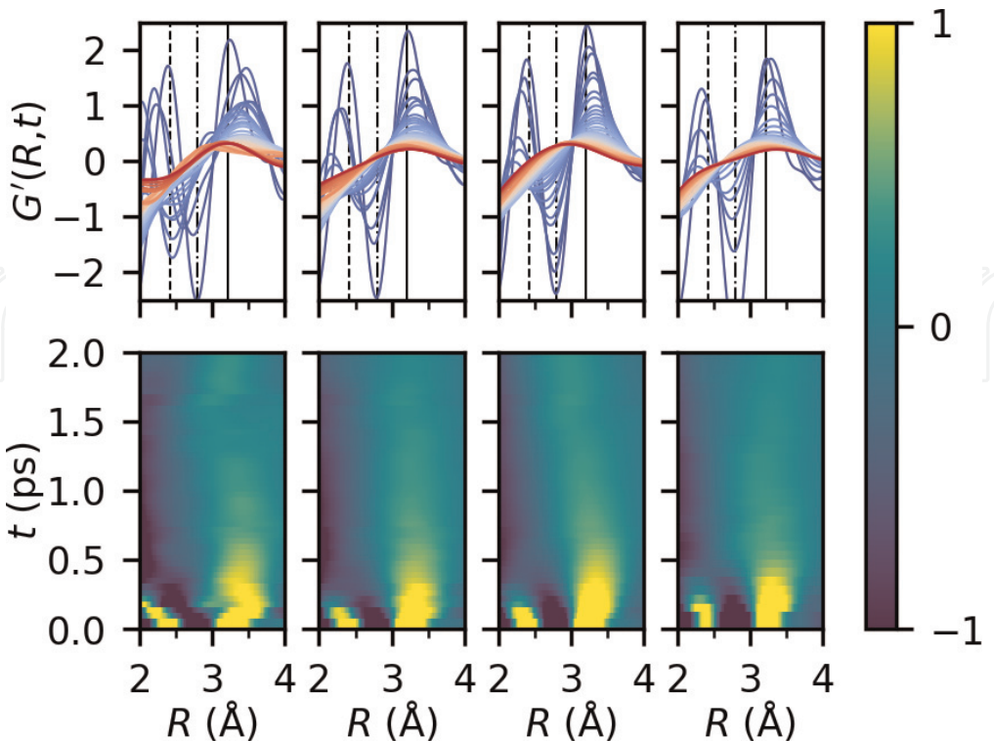

Figure 7.
One-dimensional profiles of $\boldsymbol{G}_{w-s}(\boldsymbol{r},\boldsymbol{t})$ for 0 < t < 2 ps and their intensity maps. The molality of sample is 0.75, 1.5, 2.26, and 3.0 mol/kg from the left to the right. The solid lines, dashed lines, and the dash-dotted lines in the top figures represent R = 3.21 Å (R_{O_2-} + R_{Cl-}), R = 2.42 Å (R_{O_2-} + R_{Na+}), and R = 2.8 Å (R_{O_2-} + R_{O_2-}), respectively.

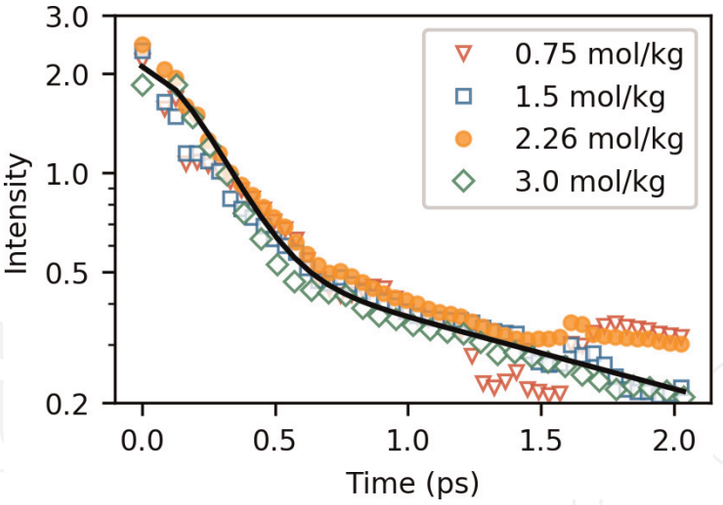

Figure 8.
Time evolution of peak height at around R = 3.21 Å. the solid line shows the result of fitting using two (compressed) exponential functions (Eq. (12)) [25].

As shown in **Figure 5**, the height of the first peak of the van Hove function is reduced by salt. The time dependence of the area of the first peak above $G(r, t) = 1$, shown in **Figure 6**, demonstrates that the addition of salt increases the slow decaying component. Furthermore it is possible to decompose the van Hove function to that of the water–water correlation, $G_{\text{w-w}}$, and that of the water-salt correlation, $G_{\text{w-s}}$,

$$G(r,t) = w_{w-w}G_{w-w}(r,t) + w_{w-s}G_{w-s}(r,t), \tag{12}$$

where $w_{\text{w-w}}$ and $w_{\text{w-s}}$ are the X-ray scattering weight for each component. The salt-salt correlation was neglected because the concentration of salt was low. If we assume that $G_{\text{w-w}}$ is the same as for pure water, we can determine $G_{\text{w-s}}$ from Eq. (12). As shown in **Figure 7**, $G_{\text{w-s}}$ is almost the same for all concentrations. The decay of the area of the sub-peak at 3.2 Å, corresponding to the Cl-O distance, is also the same for all concentrations as shown in **Figure 8**, proving the effect of salt on dynamics is local.

4. Limitations of the method

For the determination of the van Hove function, the current setup of IXS is ideally suited to the study of local dynamics in the time scale of 0.1–2 ps and length scale up to 5 Å. The energy resolution ($\sim$ 1.5 meV) sets the long-time limit to 2 ps. The effect of resolution is mitigated by the data analysis, by correcting the intermediate function for resolution,

$$F(Q,t) = F_{obs}(Q,t)/F_{res}(Q,t), \tag{13}$$

where $F_{res}(Q, t)$ is the Fourier transformation (Eq. (3)) of the energy resolution function. However, when $F_{res}(Q, t)$ becomes too small at long t, this correction is no longer sufficient. This represents a severe limitation for the IXS-derived van Hove function. To go beyond this limit, we have to resort either to neutron scattering which offers better energy resolution or to develop the method of X-ray photon correlation spectroscopy (XPCS) with free-electron X-ray laser [26]. At the

moment, because the method was only recently proven to be feasible, there are many low-hanging fruits which we are busy collecting.

5. Concluding remarks

As the instrumentation for IXS is improved, it became possible to carry out many Q-E scans in a relatively short time, covering wide Q-E space. This enables us to convert the dataset of the dynamic structure factor $S(Q, E)$ into the van Hove function $G(r, t)$ which describes dynamics in real space and time. This new capability allows us to visualize local dynamics directly rather than through the modeling for $S(Q, E)$. Even though the van Hove function is just the Fourier transform, in order to determine it, we have to measure $S(Q, E)$ over a wide Q-E space, which forces us to collect much more information than we normally do. This alone brings us to a new territory. Furthermore, by visualizing it, we gain much intuition. For instance, the behavior of the first and second peaks of water shown in **Figure 3** was totally unexpected. Only after seeing it, we understand right away what this means, but no one would have anticipated it before it is seen. It is fully expected that such surprises will occur when this approach is applied further to the study of local dynamics in liquids, glasses, and soft matter in general.

Acknowledgements

The results reviewed in this article were obtained through the extraordinary effort and dedication by the team members of the author, W. Dmowski, T. Iwashita, and Y. Shinohara, in particular. He is also grateful to A. Q. R. Baron for his invaluable help during the experiment at SPring-8. This work was supported by the Department of Energy, Office of Science, Basic Energy Sciences, Materials and Science and Engineering Division.

Conflict of interest

The author declares no conflict of interest, financial or otherwise.

Author details

Takeshi Egami[1,2]

1 University of Tennessee, Knoxville, TN, USA

2 Oak Ridge National Laboratory, Oak Ridge, TN, USA

*Address all correspondence to: egami@utk.edu

References

[1] Arbe A, Colmenero J, Farago B, Monkenbusch M, Buchenau U, Richter D. Intermediate length scale dynamics in glass forming polymers: Coherent and incoherent quasielastic neutron scattering results on polyisobutylene. Chemical Physics. 2003;**292**:295-309

[2] Novikov VN, Schweizer KS, Sokolov AP. Coherent neutron scattering and collective dynamics on mesoscale. The Journal of Chemical Physics. 2013;**138**: 164508

[3] Baron AQR. High-resolution inelastic X-ray scattering I: Context, spectrometers, samples, and superconductors. In: Synchrotron Light Sources and Free-Electron Laser. Switzerland: Springer International Publishing; 2015

[4] Baron AQR, Tanaka Y, Goto S, Takeshita K, Matsushita T, Ishikawa T. Journal of Physics and Chemistry of Solids. 2000;**61**:461-465

[5] Mason TE, Abernathy D, Anderson I, Ankner J, Egami T, Ehlers G, et al. The spallation neutron source in oak ridge: A powerful tool for materials research. Physica B. 2006;**385**:955-960

[6] Scopigno T, Ruocco G. Microscopic dynamics in liquid metals: The experimental point of view. Reviews of Modern Physics. 2005;**77**:881-933

[7] Egami T, Billinge SJL. Underneath the Bragg Peaks: Structural Analysis of Complex Materials; 2nd ed., Pergamon Materials Series Vol. 16. Oxford, UK: Pergamon Press, Elsevier Ltd.; 2012

[8] Lovesey SW. Theory of Neutron Scattering from Condensed Matter. Oxford, UK: Oxford University Press; 1984

[9] Mezei F, Knaak W, Farago B. Neutron spin-echo study of dynamic correlations near liquid-glass transition. Physica Scripta. 1987;**T19B**: 363-368

[10] Richter D, Monkenbusch M, Arbe A, Colmenero J. Neutron spin echo in polymer systems. Advances in Polymer Science. 2005;**174**:1-221

[11] Ruta B, Baldi G, Chuskin Y, Ruffle B, Cristoflini L, Fonatan A, et al. Revealing the fast atomic motion of network glasses. Nature Communications. 2014;**5**:3939

[12] Van Hove L. Correlation in space and time and born approximation scattering in systems of interacting particles. Physics Review. 1954;**95**:249-262

[13] Dahlborg U, Gudowski W, Davidovic M. Van Hove correlation functions from coherent neutron inelastic scattering. Journal of Physics: Condensed Matter. 1989;**1**:6173-6179

[14] Iwashita T, Wu B, Chen W, Tsutsui S, Baron AQR, Egami T. Seeing real-space dynamics of liquid water through inelastic X-ray scattering. Science Advances. 2017;**3**:e1603079

[15] Kawakita Y, Kikuchi T, Inamura Y, Tahara S, Maruyama K, Hanashima T, et al. Anomaly of structural relaxation in complex liquid metal of bismuth—Dynamic correlation function of coherent quasi-elastic neutron scattering. Physica B: Condensed Matter. 2018;**551**:291-296

[16] Vineyard GH. Scattering of slow neutrons by a liquid. Physics Review. 1958;**110**:999-1010

[17] de Gennes PG. Liquid dynamics and inelastic scattering of neutrons. Physica. 1959;**25**:825-839

[18] Wu B, Iwashita T, Egami T. Atomic dynamics in simple liquid: De Gennes

narrowing revisited. Physical Review Letters. 2018;**120**:135502

[19] Cargill GS III. Structure of metallic alloy glasses. Solid State Physics. 1975; **30**:227-320

[20] Sette F, Ruocco G, Krisch M, Masciovecchio C, Verbeni R, Bergmann U. Transition from normal to fast sound in liquid water. Physical Review Letters. 1996;**77**:83-86

[21] Scopigno T, Balucani U, Ruocco G, Sette F. Inelastic X-ray scattering and the high-frequency dynamics of disordered systems. Physica B. 2002; **318**:341-349

[22] Iwashita T, Nicholson DM, Egami T. Elementary excitations and crossover phenomenon in liquids. Physical Review Letters. 2013;**110**:205504

[23] Shinohara Y, Dmowski W, Iwashita T, Wu B, Ishikawa D, Baron AQR, et al. Viscosity and real space molecular motion of water: Observation with inelastic X-ray scattering. Physical Review E. 2018;**98**:022604

[24] Egami T, Shinohara Y. Dynamics of water in real space and time. Molecular Physics. 2019. DOI: 10.1080/ 00268976.2019.1649488. accepted for publication on May 8

[25] Shinohara Y, Dmowski W, Iwashita T, Ishikawa D, AQR B, Egami T. Local correlated motions in aqueous solution of sodium chloride. Physical Review Materials. 2019;**3**:065604

[26] Roseker W, Hruszkewycz SO, Lehmkühler F, Walther M, Shulte-Schrepping H, Lee S, et al. Towards ultrafast dynamics with split-pulse X-ray photon correlation spectroscopy at free electron laser sources. Nature Communications. 2018;**9**:1704